

A Subspace Approach for Extracting Signals Highly Corrupted by Colored Noise

Mohd Zuki Yusoff and Fawnizu Azmadi Hussin

Universiti Teknologi PETRONAS, Bandar Seri Iskandar, 31750 Tronoh, Perak, MALAYSIA

Summary

Estimating a signal which is buried inside colored noise is challenging since significant amount of the noise frequencies with considerable or higher power (signal-to-noise ratio, SNR, being less than 0 dB) reside in the same band as that of the desired waveform. An optimization and eigen-decomposition-based subspace approach has been investigated and tested to estimate signals which are highly corrupted by colored noise; Hu and Loizou [Y. Hu and P. C. Loizou, "A Generalized Subspace Approach for Enhancing Speech Corrupted by Colored Noise," IEEE Transactions on Speech and Audio Processing, vol. 11, no. 4, pp. 334-341, July 2003] introduced a non-symmetric basis matrix to be eigen-decomposed into its corresponding eigenvalue and eigenvector matrices; the generated eigenvector matrix is supposed to simultaneously diagonalize both the clean speech and noise covariance matrices. They also reported that the utilization of the eigenvector and eigenvalue matrices in the time-domain constrained estimator would result in the optimal estimation of speech corrupted by colored noise. Here we critically examine these matrices and contend that the presented eigen-based equations are mathematically incorrect. The eigenvectors of the proposed basis matrix produce perfectly diagonal eigenvalues for the noise covariance matrix; however, the generated eigenvalues are not the degenerate identity matrix as claimed by the authors. An alternative solution by means of a modified gain matrix is proposed to rectify the mathematical inconsistencies. For validation purposes, the pre- and post-modified algorithms have been assessed in their abilities to extract visual evoked potentials (VEPs) that are corrupted by colored electroencephalogram (EEG) noise—SNR values can be as low as -10 dB in real clinical environments. The simulation results produced by the post-modified SSA2 algorithm, show a higher degree of consistencies in detecting the VEP's P100, P200, and P300 peaks, in comparisons to the pre-modified SSA1 method. Moreover, the results of the real patient data confirm the superiority of SSA2 over SSA1 in estimating VEP's P100 latencies, which are used by doctors to assess the conduction of electrical signals from the subjects' retinas to the visual cortex parts of their brains.

Keywords:

Speech signals, evoked potentials, signal subspace, time-domain estimator, colored noise, latencies, blind signal separators.

1. Introduction

In any signal enhancement methods, researchers normally

seek to filter and reduce noise as much as possible without compromising the integrity of the desired signal. In general, subspace-based (principal component analysis) techniques have the capability to recover and preserve the quality of the desired signal, if properly exploited.

Principal component analysis, originating in work by Karl Pearson around the turn of the last century and further developed in 1930s by Harold Hotelling, consists of finding an orthogonal transformation of the original – stochastic – variables to a new set of uncorrelated variables, which are derived in a decreasing order of importance. These so-called principal components are linear combinations of the original variables such that their first few components will account for most of the variations in the original data, effectively reducing the dimensionality of the data [1].

Any subspace technique makes use of second order statistics, namely the correlation or covariance matrices of the pertinent signal vectors. Next, a subspace technique utilizes eigenvectors, eigenvalues and diagonalization which constitute the eigendecomposition of a correlation or covariance matrix. Normally, the eigenvalue decomposition operation is closely related with the Karhunen-Loeve Transform (KLT) approach [2]. However, it has been shown in [3] that a signal subspace approach based on non-unitary (non-KLT) transformation is still possible, providing that great care is taken in the selection of a basis matrix, the formation of transform and inverse transform matrices from the resulting non-unitary eigenvectors, and the choice of a matrix or matrices to be decorrelated.

In the last ten years, subspace filtering techniques have frequently been used in spectrum estimation [4, 5], system identification [6, 7], digital speech processing [8, 9], and later in evoked potential estimation [3], due to its power and flexibility. One of the most notable subspace-based techniques is the one developed by Ephraim and Van Trees [8] to extract a speech signal that is contaminated by white noise. Based on this work, Rezayee and Gazor [10] extended the time and spectrum domain constrained

methods of [8] to deal with colored noise, without using a pre-whitening stage. Reference [10] applied a Karhunen-Loève transform (KLT) approach by introducing a unitary “common diagonalizing eigenvector matrix” (CDEM) derived from the eigendecomposition of the observed signal covariance matrix.

Further, [10] acknowledged that the generated CDEM approximately diagonalizes both the covariance matrices of the clean signal and noise process. However, [11] argued that the selected CDEM would result in a sub-optimal speech estimator since both the clean signal and noise covariance matrices are not fully diagonalized. Accordingly, [11] aimed at producing an optimal speech enhancer by suggesting explicit pre-whitening and proposing a non-KLT, and therefore a non-unitary CDEM (based on the eigendecomposition of a non-symmetric basis matrix) that would jointly diagonalize the signal and noise covariance matrices.

In our preliminary investigations, we applied and evaluated the signal subspace principles in [10, 11] above in the estimation of visual evoked potentials (VEPs) from the brain. As far as VEP estimation is concerned, the approach in [10] actually outperforms that in [11] even though the method suggested by [10] is sub-optimal. Upon closer inspections the formulas proposed by [11] contain inconsistencies.

In this paper, we review the generic signal subspace method based on a time-domain-constrained (TDC) approach [8] and thoroughly evaluate the estimator proposed by [11] to assess its mathematical soundness and suggest some changes to rectify the shortcomings of the equations. Subsequently, we compare the performance of the pre- and post-modified algorithms in the estimation of visual evoked potential (VEP) signals.

The paper is organized as follows. The general TDC signal subspace technique is clearly explained in Section 2. The eigendecomposition method proposed by [11] is briefly described in Section 3. In Section 4, we derive the correct formulas for the TDC estimator, modifying the introduced gain matrix of [11]. Next, Section 5 describes the results of VEP latency estimation—using our modified signal subspace approach and the technique of [11]—in simulated and real clinical environments. Last, Section 6 concludes the paper.

To ensure common understanding and consistencies, all mathematical symbols, operators, notations and terminologies used are in compliance with the acceptable

styles and conventions normally adopted worldwide. Lower case **boldface** characters will generally refer to vectors. Upper case **BOLDFACE** characters will generally refer to matrices. Vector or matrix transposition will be denoted using $(\cdot)^T$, and $\mathfrak{R}^{M \times M}$ denotes the real vector space of $M \times M$ dimensions.

2. Model Development

2.1 Signal Model

In developing a mathematical expression for extracting the signal, the following model is defined.

$$\mathbf{y}(k) = \mathbf{x}(k) + \mathbf{n}(k) \quad (1)$$

where, the lowercase k is the discrete time index; $\mathbf{y}(k) \in \mathfrak{R}^M$ is the M -dimensional vector of the corrupted (noisy) signal; $\mathbf{x}(k) \in \mathfrak{R}^M$ is the M -dimensional vector of the original (clean) signal; $\mathbf{n}(k) \in \mathfrak{R}^M$ is the M -dimensional vector of the additive colored noise which is assumed to be uncorrelated with $\mathbf{x}(k)$. Next, $\mathbf{H}(k) \in \mathfrak{R}^{M \times M}$ is defined as the $M \times M$ -dimensional matrix of the signal time-domain constrained linear estimator. Further, $\hat{\mathbf{x}}(k) \in \mathfrak{R}^M$ is defined as the M -dimensional vector of the estimated signal. Afterwards, any vectors or matrices that appear without a time index should be visualized as having the ks as their time indexes.

2.2 Estimated Signal

The estimated (speech or any other) signal $\hat{\mathbf{x}}$ is related to \mathbf{H} and \mathbf{y} in the following way [8]:

$$\hat{\mathbf{x}} = \mathbf{H}_{opt} \cdot \mathbf{y} \quad (2)$$

The estimated signal $\hat{\mathbf{x}}$ will never be exactly equal to the original (clean) signal \mathbf{x} . In other words, errors will inevitably be produced in the estimated signal. Basically, the system equation in Eq. (2) is to minimize a specified error criterion, which is the ultimate measure of the signal estimation performance criterion. As such, the error signal $\boldsymbol{\varepsilon}$ obtained by this estimation is given by [8]:

$$\begin{aligned} \boldsymbol{\varepsilon} &= \hat{\mathbf{x}} - \mathbf{x} = (\mathbf{H} - \mathbf{I})\mathbf{x} + \mathbf{H}\mathbf{n} \\ &= \boldsymbol{\varepsilon}_x + \boldsymbol{\varepsilon}_n, \quad \boldsymbol{\varepsilon}_x = (\mathbf{H} - \mathbf{I})\mathbf{x} \text{ and } \boldsymbol{\varepsilon}_n = \mathbf{H}\mathbf{n} \end{aligned} \quad (3)$$

where $\boldsymbol{\varepsilon}_x$ represents the speech distortion and $\boldsymbol{\varepsilon}_n$ represents the residual noise. The energies of the signal distortion

$$\begin{aligned} \bar{\boldsymbol{\varepsilon}}_x^2 &= \text{tr}\left(\mathbb{E}\left\{\boldsymbol{\varepsilon}_x \boldsymbol{\varepsilon}_x^T\right\}\right) = \text{tr}\left((\mathbf{H} - \mathbf{I})\mathbf{R}_x(\mathbf{H} - \mathbf{I})^T\right), \\ \mathbf{R}_x &= \text{desired signal covariance matrix} \end{aligned} \quad (4)$$

and the energies of the residual noise

$$\bar{\epsilon}_n^2 = \text{tr}(\mathbb{E}\{\epsilon_n \epsilon_n^T\}) = \text{tr}(\mathbf{H}\mathbf{R}_n\mathbf{H}^T), \quad (5)$$

$\mathbf{R}_n = \text{colored noise covariance matrix}$

lead to the total residual energies

$$\bar{\epsilon}^2 = \bar{\epsilon}_x^2 + \bar{\epsilon}_n^2 \quad (6)$$

Our main goal is to minimize both the unwanted energies so that a minimal error signal is obtained. The challenge is when speech signal distortion is at its lowest, noise residues will be at its highest; on the other hand, if noise is fully minimized, distortion will be at its greatest. Therefore, a good balance needs to be set so that the noise residues can be reasonably minimized without introducing significant distortion to the processed signal.

2.3 Estimator Optimization

Now, the aim is to design a linear estimator \mathbf{H} that minimizes the speech signal distortion over all linear filters. This can be achieved by maintaining the residual noise within a permissible level. Mathematically, the optimum linear estimator \mathbf{H}_{opt} with time-domain constraints on the residual noise is formulated as [8]:

$$\mathbf{H}_{opt} = \min_{\mathbf{H}} \bar{\epsilon}_x^2 \quad \text{subject to: } \bar{\epsilon}_n^2 \leq M\sigma^2 \quad (7)$$

where M is the dimension of the noisy vector space and σ^2 is a positive constant noise threshold level. The σ^2 in Eq. (7) dictates the amount of the residual noise allowed to remain in the linear estimator. Next, the Lagrangian function in association with the ‘‘Kuhn-Tucker necessary conditions for constrained minimization’’ [8] are applied to Eq. (7) to obtain \mathbf{H}_{opt} . The formed Lagrangian function can be expressed as:

$$\mathbf{L}(\mathbf{H}, \mu) = \bar{\epsilon}_x^2 + \mu(\bar{\epsilon}_n^2 - M\sigma^2) \quad (8)$$

It follows that the filter matrix \mathbf{H} is a stationary feasible point if it satisfies the following gradient equation $\nabla_{\mathbf{H}}\mathbf{L}(\mathbf{H}, \mu) = 0$:

$$\begin{aligned} \frac{\partial \mathbf{L}(\mathbf{H}, \mu)}{\partial \mathbf{H}} &= \frac{\partial}{\partial \mathbf{H}} [\bar{\epsilon}_x^2 + \mu(\bar{\epsilon}_n^2 - M\sigma^2)] = 0 \\ \Rightarrow \frac{\partial}{\partial \mathbf{H}} [\text{tr}(\mathbf{H} - \mathbf{I})\mathbf{R}_x(\mathbf{H} - \mathbf{I})^T] &+ \\ \frac{\partial}{\partial \mathbf{H}} [\mu \text{tr}(\mathbf{H}\mathbf{R}_n\mathbf{H}^T)] &= 0 \\ \Rightarrow \mathbf{H}(\mathbf{R}_x + \mu\mathbf{R}_n) - \mathbf{R}_x &= 0 \end{aligned} \quad (9)$$

Subsequently, the gradient equation in Eq. (9) can be

solved to be

$$\mathbf{H} = \mathbf{R}_x(\mathbf{R}_x + \mu\mathbf{R}_n)^{-1} \quad (10)$$

Other Kuhn-Tucker necessary conditions to be fulfilled are

$$\mu(\bar{\epsilon}_n^2 - M\sigma^2) = 0 \quad (11)$$

for

$$\mu \geq 0 \quad (12)$$

The values for μ and σ^2 satisfying Eqs. (11) and (12) need to be determined. Equation (11) can be simplified to yield

$$\bar{\epsilon}_n^2 = M\sigma^2 \quad (13)$$

The following expression for σ^2 is obtained by equating Eq. (13) with Eq. (5):

$$\begin{aligned} \bar{\epsilon}_n^2 &= M\sigma^2 = \text{tr}(\mathbf{H}\mathbf{R}_n\mathbf{H}^T) \\ \Rightarrow \sigma^2 &= \frac{1}{M} \text{tr}(\mathbf{H}\mathbf{R}_n\mathbf{H}^T) \end{aligned} \quad (14)$$

Equation (14) is more meaningful if a relationship between σ^2 and μ can be established. This is achieved by replacing \mathbf{H} computed in Eq. (10) into Eq. (14).

$$\sigma^2 = \frac{1}{M} \text{tr}(\mathbf{R}_x^2(\mathbf{R}_x + \mu\mathbf{R}_n)^{-2}\mathbf{R}_n) \quad (15)$$

One issue that arises from Eq. (15) is whether to first specify the permissible level of residual noise σ^2 , or the Lagrange multiplier μ . The first approach is to specify σ^2 in Eq. (15) and calculate μ from it. On the other hand, μ can be carefully chosen so that σ^2 can be calculated. Therefore, μ which satisfies Eq. (15) also satisfies Eqs. (11) and (12). Hence, μ must also be the Lagrange multiplier for the time-domain-constrained (TDC) optimization problem of Eq. (7).

2.4 Eigendecomposition of Estimator Parameters

The filter matrix \mathbf{H} stated in Eq. (10) functions as a fixed filter, which performs well to estimate the desired signal for a relatively high SNR value. As the SNR degrades, it is desirable if \mathbf{H} can be adjusted accordingly to minimize the colored noise residues while keeping the desired signal distortion at a minimal level.

One possible way to achieve an adjustable filter matrix \mathbf{H} is by taking the eigendecomposition of its \mathbf{R}_x and \mathbf{R}_n terms. When \mathbf{R}_x and \mathbf{R}_n are represented by their respective eigenvectors and eigenvalues, the fixed filter matrix \mathbf{H} then

becomes adjustable. If the dimension of the \mathbf{R}_x eigenvalues is not lowered, the filter \mathbf{H} functions exactly as that denoted in Eq. (10) — keeping signal distortion to its very minimum and noise energy to its maximum.

When the dimension of \mathbf{R}_x is lowered to a certain rank, the filter \mathbf{H} will eliminate certain noise portions. If a proper dimension of the \mathbf{R}_x eigenvalues is used, the component in the “noise only” subspace will get nulled. The component that remains available at the output of the filter \mathbf{H} is the wanted signal from the “signal” subspace. Of course, the wanted signal may not be completely free from noise since the “signal” subspace is actually a “signal plus noise” subspace. Nevertheless, the wanted signal is now clearly visible as the SNR value gets improved due to the subspace filtering technique.

3. Hu and Loizou's Eigendecomposition Approach

Hu and Loizou [11] suggested the usage of a common diagonalizing eigenvector matrix (CDEM) that simultaneously and fully diagonalizes the signal and noise covariance matrices. For this, [11] stated that there exists a basis matrix $\mathbf{\Psi}$ that can supposedly produce the required CDEM, satisfying the following equations:

$$\mathbf{\Psi V} = \mathbf{VA} \tag{16}$$

$$\mathbf{V}^T \mathbf{R}_x \mathbf{V} = \mathbf{A}_x = \mathbf{A} \tag{17}$$

$$\mathbf{V}^T \mathbf{R}_n \mathbf{V} = \mathbf{A}_n = \mathbf{I} \tag{18}$$

where \mathbf{A} and \mathbf{V} are, respectively, the eigenvalue and non-unitary eigenvector matrices of $\mathbf{\Psi}$; correspondingly, \mathbf{A}_x and \mathbf{A}_n are the eigenvalues of \mathbf{R}_x and \mathbf{R}_n . In turn, $\mathbf{\Psi}$ was set to $\mathbf{R}_n^{-1} \mathbf{R}_x$ (i.e., $\mathbf{\Psi} = \mathbf{R}_n^{-1} \mathbf{R}_x$). Applying Eqs. (16), (17) and (18) to (10), [11] simplified their optimal linear estimator \mathbf{H}_{SSAI} as

$$\begin{aligned} \mathbf{H}_{SSAI} &= \mathbf{V}^{-T} \mathbf{A}_x (\mathbf{A}_x + \mu \mathbf{I})^{-1} \mathbf{V}^T = \mathbf{V}^{-T} \mathbf{G} \mathbf{V}^T \\ &= \mathbf{R}_n \mathbf{V} \mathbf{G} \mathbf{V}^T, \text{ gain matrix } \mathbf{G} = \mathbf{A}_x (\mathbf{A}_x + \mu \mathbf{I})^{-1} \end{aligned} \tag{19}$$

Based on Eq. (2), the estimated (speech) signal was then calculated as [11]

$$\begin{aligned} \hat{\mathbf{x}}_{SSAI} &= \mathbf{H}_{SSAI} \bullet \mathbf{y} = \mathbf{V}^{-T} \mathbf{G} \mathbf{V}^T \bullet \mathbf{y} \\ &= \mathbf{R}_n \mathbf{V} \mathbf{G} \mathbf{V}^T \bullet \mathbf{y} \quad \text{where } \mathbf{G} = \mathbf{A}_x (\mathbf{A}_x + \mu \mathbf{I})^{-1} \end{aligned} \tag{20}$$

Upon closer scrutiny, the following facts have been revealed:

1. Equation (16) holds true. In fact, this equation will hold true for the eigendecomposition of any matrix. It is to be

noted that the eigendecomposition of $\mathbf{\Psi} = \mathbf{R}_n^{-1} \mathbf{R}_x$ results in a non-unitary eigenvector \mathbf{V} .

2. Equation (17) holds true, partly. It produces fully diagonal "non-unity" eigenvalues of \mathbf{R}_x given as

$$\begin{aligned} \mathbf{V}^T \mathbf{R}_x \mathbf{V} &= \mathbf{A}_x \neq \mathbf{A}, \text{ and} \\ \mathbf{V}^{-T} \mathbf{A}_x \mathbf{V}^{-1} &= \mathbf{R}_x \end{aligned} \tag{21}$$

However, it can be observed from Eq. (21) that \mathbf{A}_x is totally different from \mathbf{A} .

3. Equation (18) does not hold true. It actually produces fully diagonal eigenvalues of \mathbf{R}_n given as

$$\begin{aligned} \mathbf{V}^T \mathbf{R}_n \mathbf{V} &= \mathbf{A}_n \neq \mathbf{I}, \\ \mathbf{V}^{-T} \mathbf{A}_n \mathbf{V}^{-1} &= \mathbf{R}_n, \text{ and} \\ \mathbf{V}^{-T} \mathbf{I} \mathbf{V}^{-1} &\neq \mathbf{R}_n \end{aligned} \tag{22}$$

It is obvious that \mathbf{A}_x and \mathbf{A} in Eq. (21) are not equal to each other, and \mathbf{A}_n in Eq. (22) is not an identity matrix \mathbf{I} as stated (by [11]) in Eqs. (17) and (18), respectively.

Equation (19) and subsequently (20) are valid if and only if Eqs. (17) and (18) are valid. However, since Eq. (18) is invalid, the algorithm proposed by [11] is arguable. Their claim in producing an optimal (speech) signal enhancer by introducing a non-unitary CDEM is flawed by the claim that \mathbf{A}_x equals to \mathbf{A} , and by assuming that \mathbf{A}_n in Eq. (18) is equal to the identity matrix \mathbf{I} .

4. Corrections to Hu and Loizou's Eigendecomposition

4.1 Proposed Modifications to SSA1 Algorithm

The flaws in [11] can be easily corrected by substituting \mathbf{R}_x and \mathbf{R}_n in Eq. (10) with their corresponding expressions, as stated in Eqs. (21) and (22), respectively. It follows that the gain matrix \mathbf{G} in Eq. (19) is actually

$$\mathbf{G} = \mathbf{A}_x (\mathbf{A}_x + \mu \mathbf{A}_n)^{-1} \tag{23}$$

The difference between \mathbf{G} in Eq. (23) and that in Eq. (19) is that the former has the \mathbf{A}_n term included as part of the computation. Hence, the modified estimator which makes Eq. (19) mathematically correct can be expressed as follows:

$$\begin{aligned} \mathbf{H}_{SSA2} &= \mathbf{V}^{-T} \mathbf{A}_x (\mathbf{A}_x + \mu \mathbf{A}_n)^{-1} \mathbf{V}^T \\ &= \mathbf{V}^{-T} \mathbf{G} \mathbf{V}^T, \quad \mathbf{G} = \mathbf{A}_x (\mathbf{A}_x + \mu \mathbf{A}_n)^{-1} \end{aligned} \tag{24}$$

Equation (24) leads to the following estimated signal:

$$\begin{aligned} \hat{\mathbf{x}}_{SSA2} &= \mathbf{H}_{SSA2} \bullet \mathbf{y} \\ &= \mathbf{V}^{-T} \mathbf{G} \mathbf{V}^T \bullet \mathbf{y}, \quad \mathbf{G} = \mathbf{A}_x (\mathbf{A}_x + \mu \mathbf{A}_n)^{-1} \end{aligned} \quad (25)$$

The corrupted signal \mathbf{y} in Eq. (25) is decorrelated by the non-KLT matrix \mathbf{V}^T . Then, the transformed signal is modified and enhanced by the signal subspace gain matrix \mathbf{G} . Next, the modified signal is retransformed back into the original state (at a reduced rank) by the inverse non-KLT matrix \mathbf{V}^{-T} to approximate the desired signal.

4.2 Algorithm Implementation

The proposed modified approach (i.e., SSA2) can be formulated in the following twelve steps:

- Step 1. Compute the correlation matrix of the colored noise \mathbf{R}_n , using a background noise sample, just prior to the availability of the desired signal.
- Step 2. Compute the noisy correlation matrix \mathbf{R}_y , using the observed (corrupted) sample. This is the point when both the wanted signal and colored noise are present.
- Step 3. Estimate the correlation matrix of the noiseless sample as $\mathbf{R}_x = \mathbf{R}_y - \mathbf{R}_n$.
- Step 4. Perform the eigendecomposition operation on $\mathbf{\Psi} = \mathbf{R}_n^{-1} \mathbf{R}_x$ using Eq. (16). Extract the eigenvector matrix \mathbf{V} and eigenvalue matrix \mathbf{A} from the computation.
- Step 5. Calculate \mathbf{A}_x and \mathbf{A}_n using Eqs. (21) and (22), respectively.
- Step 6. Assuming that the eigenvalues of \mathbf{A}_x are ordered as $\lambda_1 \geq \lambda_2 \geq \dots \geq \lambda_M$, estimate the dimension d of the required signal subspace as follows:

$$d = \arg \left\{ \max_{1 \leq k \leq M} \lambda_k > 0 \right\} \quad (26)$$

- Step 7. Form a diagonal matrix, \mathbf{A}_{xM} , from the largest M diagonal values of \mathbf{A}_x .
- Step 8. Correspondingly, form a diagonal matrix, \mathbf{A}_{nM} , from the largest M diagonal values of \mathbf{A}_n .
- Step 9. Form a matrix \mathbf{V}_M using eigenvectors of \mathbf{V} that correspond to the largest M eigenvalues.
- Step 10. Choose a proper value for μ as a compromise between signal distortion and noise residues. Empirically, in our VEP estimation experiments, we found that $\mu = 2$ is ideal in reducing the colored EEG noise to a certain

level, while minimizing the VEP signal distortion at the same time.

- Step 11. Compute the optimal linear estimator using Eq. (24).
- Step 12. Estimate the desired signal using Eq. (25).

5. Experiments, Results and Discussions

5.1 Simulated Data

In this subsection, the performances of the SSA2 (represented by Eq. (25)) and SSA1 (represented by Eq. (20)) in estimating the VEP signals (specifically, the P100, P200, and P300 latencies) are tested in statistical forms using artificially generated VEP signals corrupted with colored noise at different SNR values.

Artificial VEP and EEG waveforms are generated and added to each other in order to create a noisy VEP. The clean VEP $\mathbf{x}(k) \in \mathfrak{R}^M$, is generated by superimposing J Gaussian functions [12], each of which having a different amplitude (A), variance (σ^2) and mean (μ) as given by the following equation:

$$\mathbf{x}(k) = \left[\sum_{n=1}^J \mathbf{g}_n(k) \right]^T \quad (27)$$

where $\mathbf{g}_n(k) = [g_{n1}, g_{n2}, \dots, g_{nM}]$, for $k = 1, 2, \dots, M$, with the individual g_{nk} given as

$$g_{nk} = \frac{A_n}{\sqrt{2\pi\sigma_n^2}} e^{-\frac{(k-\mu_n)^2}{2\sigma_n^2}} \quad (28)$$

The values for A_n , σ_n and μ_n for each \mathbf{g}_n vector are experimentally tweaked to create precise peaks (i.e., latencies) with progressively descending amplitudes at 100, 200, and 300 ms simulating the real P100, P200 and P300, respectively.

The pre-stimulation EEG colored noise $\mathbf{e}(k)$ is generated using autoregressive (AR) model [13, 14, 15] given by the following equation.

$$\begin{aligned} \mathbf{e}(k) &= 1.5084\mathbf{e}(k-1) - 0.1587\mathbf{e}(k-2) - \\ &0.3109\mathbf{e}(k-3) - 0.0510\mathbf{e}(k-4) + \mathbf{u}(k) \end{aligned} \quad (29)$$

where $\mathbf{u}(k)$ is the input driving noise of the AR filter and $\mathbf{e}(k)$ is the filter output. The artificial post-stimulation EEG noise \mathbf{n} is generated by changing the variance of \mathbf{e} . Since noise is assumed to be additive, the artificially-corrupted VEP signal \mathbf{y} is then produced by adding together \mathbf{x} and \mathbf{n} .

As a preliminary illustration, Fig. 1(a) below shows a sample of artificially generated VEP according to Eqs. (27) and (28)—showing realistically simulated amplitudes and peaks precisely at 100 ms (P100), 200 ms (P200) and 300 ms (P300); a noisy VEP at SNR = -6 dB; and extracted VEPs using both the SSA2 and SSA1 techniques. Further, Figs. 1(b) and 1(c) show the outcomes of the simulated experiments at SNRs equal to -8 and -10 dB, respectively.

From Fig. 1(a), it can be observed that SSA2 estimates the latencies of P100, P200 and P300 components as 106, 205 and 297 ms, respectively. The pertinent latencies produced by SSA1 are 108 (for P100), 204 (for P200) and 295 ms (for P300). From Fig. 1(b), SSA2 generates 99, 192 and 314 ms, while SSA1 produces 105, 192 and 326 ms of latencies. Further from Fig. 1(c), SSA2 estimates the P100, P200 and P300 components as 98, 205 and 320 ms, respectively. The pertinent latencies produced by SSA1 are 98 (for P100), 212 (for P200) and 328 ms (for P300). These early observations indicate that SSA2 manages to extract and bring the P100, P200 and P300 peaks much closer to their reference values (i.e., 100, 200 or 300 ms) compared to SSA1.

To compare the performances of the two algorithms in statistical forms, the SNR was varied from 0 to -10 dB and the algorithms were run 500 times for each SNR value. Failure rate and average errors are used in this paper as vital test tools in assessing the performance of the filters in single-trial estimation of VEPs.

To measure failure rate, visual inspections were performed to judge whether or not the estimators' processed waveforms are acceptable. The three highest peaks within 100 ± 10 , 200 ± 10 and 300 ± 10 ms are considered as the wanted P100, P200 and P300 components. Any trial is noted as a failure with respect to a certain peak if the waveform fails to show clearly the pertinent peak within the stated ± 10 ms tolerance. The failure rate for each algorithm with respect to a certain peak and SNR is expressed in terms of a percentage. It is calculated according to the following formula:

$$\text{failure rate} = \frac{\text{number of failures}}{N} \times 100\% \quad (30)$$

where N is the number of runs (trials) per SNR which in this case equals to 500.

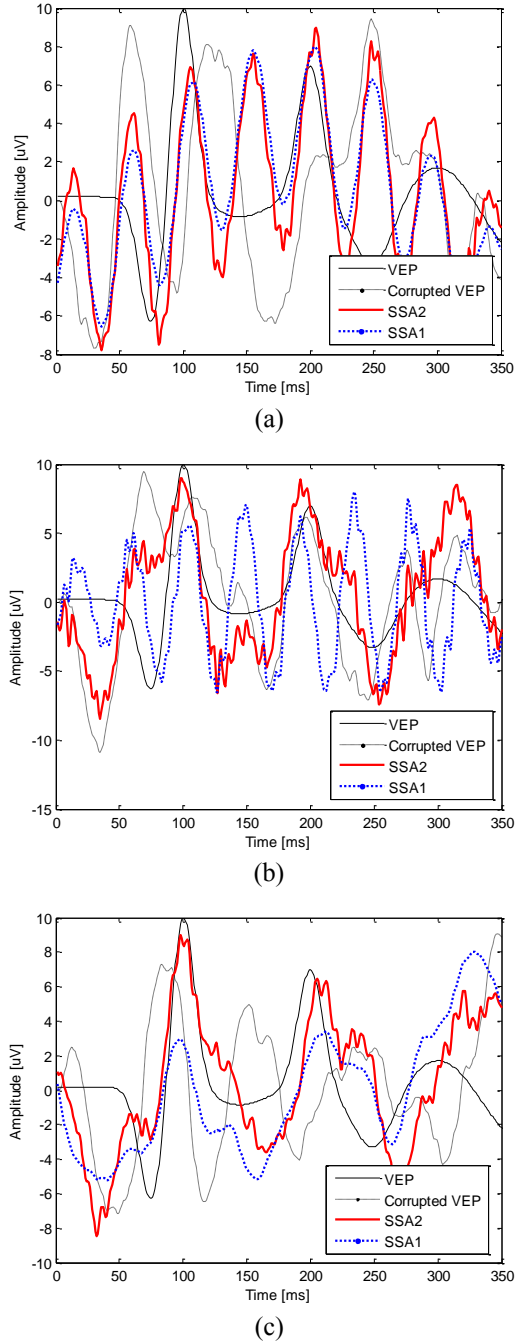


Fig. 1 Simulated waveforms of clean and noisy VEPs, and extracted VEPs using SSA2 and SSA1, at SNR equal to (a) -6 dB; (b) -8 dB; and (c) -10 dB.

The average error in estimating P100 is obtained as follows:

$$\bar{\varepsilon}_{P100} = \frac{\left(\sum_{i=1}^N |\hat{t}_{P100}(i) - 100| \right)}{N} \quad (31)$$

where $\hat{t}_{P100}(i)$ is the estimated latency (for each run) of the P100 in milliseconds. The average errors for P200 and P300 components can be calculated in the same way. The failure rates and average errors for the simulated data are shown in Table 1 below.

Table 1: The failure rate and average errors of SSA2 and SSA1 as a function of SNR.

SNR [dB]	Failure Rate [%]			Average error		
	Peak	SSA2	SSA1 [11]	Peak	SSA2	SSA1 [11]
0	P100	0.2	13.2	P100	3.8	6.1
	P200	0.6	23.6	P200	3.9	8.9
	P300	51.8	53.4	P300	12.1	14.5
-2	P100	0	14.4	P100	3.8	7.3
	P200	3.8	27.0	P200	4.2	9.5
	P300	50.2	55.4	P300	12.2	15.3
-4	P100	1.0	16.8	P100	3.9	8.2
	P200	5.8	25.0	P200	4.6	8.4
	P300	48.6	57.6	P300	11.9	15.4
-6	P100	1.2	13.0	P100	3.8	6.7
	P200	8.4	31.2	P200	5.1	10.1
	P300	53.0	58.2	P300	12.8	15.1
-8	P100	2.0	16.8	P100	4.2	8.3
	P200	9.0	31.0	P200	5.2	10.1
	P300	53.8	55.8	P300	12.3	15.8
-10	P100	2.4	18.2	P100	4.2	7.9
	P200	14.4	34.2	P200	6.1	10.7
	P300	54.8	61.4	P300	12.9	16.2

From Table 1 it is clear that the proposed SSA2 algorithm outperforms SSA1 in terms of failure rates and accuracies over the considered range of SNRs. In general, both algorithms show better efficiencies in estimating the latencies of P100's than they are with the other P200 and P300 peaks.

Further, performance metrics such as peak latency mean and peak latency standard deviations are also used to gauge accuracies and precisions of the techniques under investigations. For five hundred different runs per SNR, the average of the estimated P100 peak latencies, denoted as \bar{P}_{100} , is calculated as

$$\bar{P}_{100} = \frac{\sum_{i=1}^{500} \hat{t}_{P100}(i)}{500} \quad (32)$$

where $\hat{t}_{P100}(i)$ is the individually estimated latency of the P100 peak in milliseconds. Again, the \bar{P}_{200} and \bar{P}_{300} can be determined in the same way. It is important to note that

the mean value of the P100 peak latency closer to 100 ms, may not always indicate better accuracy. Subsequently, the performance of a filter should not rely on just the average value; its performance must be judged using standard deviations.

The standard deviation of the P100 peak latencies, denoted as σ_{P100} , for the five hundred runs per SNR is calculated using

$$\sigma_{P100} = \sqrt{\frac{\sum_{i=1}^{500} (\hat{t}_{P100}(i) - \bar{t}_{P100})^2}{500 - 1}} \quad (33)$$

where $\hat{t}_{P100}(i)$ is the estimated latencies of the P100 in milliseconds, and \bar{t}_{P100} is the average value (in milliseconds) of the five hundred P100 data sets. Similarly, σ_{P200} or σ_{P300} can be calculated by replacing $\hat{t}_{P100}(i)$ and \bar{t}_{P100} in Eq. (33) with $\hat{t}_{P200}(i)$ and \bar{t}_{P200} , or $\hat{t}_{P300}(i)$ and \bar{t}_{P300} . Overall, the smaller the standard deviation of the estimated peak latency, the better the performance of the technique is. Specifically, the P100 (or P200, or P300) with a peak latency average closer to 100 ms (or 200 ms, or 300 ms), coupled with a narrower standard deviation indicates better performance.

The peak latency mean and standard deviations are listed in Table 2 below. From Table 2, it can be observed that SSA2 and SSA1 produce comparable mean values of the peak latencies; however, SSA2 always produces lower standard deviations. This means SSA2 performs better than SSA1.

The inclusion of the eigenvalue matrix \mathbf{A}_n in the gain matrix \mathbf{G} (Eq. 23) improves the performance of SSA2. Actually, the performance of SSA1 is relatively high; oversimplification in the original algorithm of [11] slightly affects its accuracy and precision, in comparison to the modified SSA2 method.

Table 2: The mean (in ms) of peak latencies and standard deviations (std) of SSA2 and SSA1 as a function of SNR.

SNR [dB]	SSA2			SSA1 [11]		
	Peak	Mean	Std	Peak	Mean	Std
0	P100	103.8	1.5	P100	104.8	9.3
	P200	203.6	2.7	P200	201.7	15.9
	P300	302.8	13.9	P300	301.2	18.3

-2	P100	103.9	1.8	P100	105.0	11.3
	P200	203.8	3.5	P200	201.8	14.6
	P300	301.2	15.3	P300	301.9	20.5
-4	P100	103.8	1.9	P100	105.5	12.4
	P200	203.6	4.4	P200	200.6	18.2
	P300	301.7	15.6	P300	300.9	25.4
-6	P100	104.3	3.5	P100	104.9	11.6
	P200	203.5	5.9	P200	201.7	18.5
	P300	301.9	14.5	P300	301.9	19.6
-8	P100	103.9	2.7	P100	104.9	13.7
	P200	203.3	6.1	P200	201.9	16.2
	P300	300.7	14.5	P300	300.1	23.7
-10	P100	104.2	2.8	P100	106.3	11.9
	P200	203.7	7.3	P200	201.2	16.6
	P300	301.5	15.7	P300	302.1	23.1

To further validate the performance of the SSA2 and SSA1 estimators, the next experiments will deal with real patient data. Nevertheless, the performance outcome and evidence collected in the simulated experiments above are the utmost crucial in proving the true capabilities of the filters as single-trial estimators; this is because the true forms of the individual VEPs from real patient data are not known *a priori*.

5.2 Real Patient Data

In this subsection, the accuracies of SSA2 and SSA1 as single-trial estimators of the P100 latencies, used in the objective assessment of the visual pathways from the retina to the visual cortex of the human brain, are tested. Real patient experiments were conducted at Selayang Hospital, Kuala Lumpur using RETIport32 equipment. The experiments were carried out on **normal** subjects without any neurological deficit or medication known to affect the EEG.

Subjects were asked to watch a checkerboard pattern (1° full field), the stimulus being a checker reversal ($N = 50$ stimuli). Scalp recordings were made according to the International 10/20 System, with one eye closed at any given time. The active electrode was connected to the middle of the occipital (O1, O2) area while the reference electrode was attached to the middle of the forehead.

In this paper, we will show the results for artefact-free trials of **four** subjects taken from their right eyes only; for this purpose, each subject's right eye was left open while his/her left eye was shaded by an eye patch. Each trial was pre-filtered in the range 0.1 to 70 Hz and sampled accordingly, creating 512 data points within a 333 ms span.

Each subject underwent two separate recording sessions. In the first session, eighty trials for each subject were

obtained and automatically averaged (using ensemble averaging) by the RETIport32 equipment to get the VEP signal and accordingly the latency of P100, which is the peak of interest of doctors at the Ophthalmology Department, Selayang Hospital. In general, VEP latencies such as the P100's are used by clinicians to check the integrity of the subjects' visual pathways from the retinas to the occipital cortex parts of their brains.

Since ensemble averaging (EA) is a multi-trial technique, it is expected to produce good estimation of the VEP latency that can be used as a baseline for comparing the performances of GSA and TOC.

In the second session, 333 ms (machine dependent) of recording time was allocated to capture the brain activity just before a visual stimulation was applied to the subject. The recorded data for the entire 333 ms duration pertain to the pre-stimulus EEG signal which basically describes the brain background colored noise. Then, the next 333 ms was used to record the post-stimulus waveform which comprises the VEP and post-EEG signals. These pre- and post-stimulation signals are required by the SSA2 and SSA1 algorithm.

The P100 latencies of four different subjects estimated by the single-trial SSA2 and SSA1 estimators, together with the corresponding P100 values approximated by the multi-trial ensemble averaging (EA) are shown in Figs. 2(a) through 2(d) below. Attention is given to any dominant (i.e., highest) peak(s) from 90 to 140 ms. It should be noted that any peaks that occur below 90 ms and above 140 ms are considered as noise and are therefore ignored. The results, in milliseconds, are summarized as follows:

- Fig. 2(a): EA = 99; SSA2 = 100; SSA1 = 98 ms.
- Fig. 2(b): EA = 119; SSA2 = 119; SSA1 = 118 ms.
- Fig. 2(c): EA = 108; SSA2 = 111; SSA1 = 131 ms.
- Fig. 2(d): EA = 117; SSA2 = 118; SSA1 = 120 ms.

From the results obtained, it can be stated that SSA2 outperforms SSA1 in estimating the latencies of the P100 components. The latency values generated by SSA2 are closer to those generated by EA compared to those produced by SSA1. In brief, the simulated and real data experiments exhibit the capability of the subspace-based technique such as SSA2 in VEP latency estimation. Most importantly, the results of both experiments prove higher reliabilities and higher accuracies of the proposed SSA2 algorithm over SSA1.

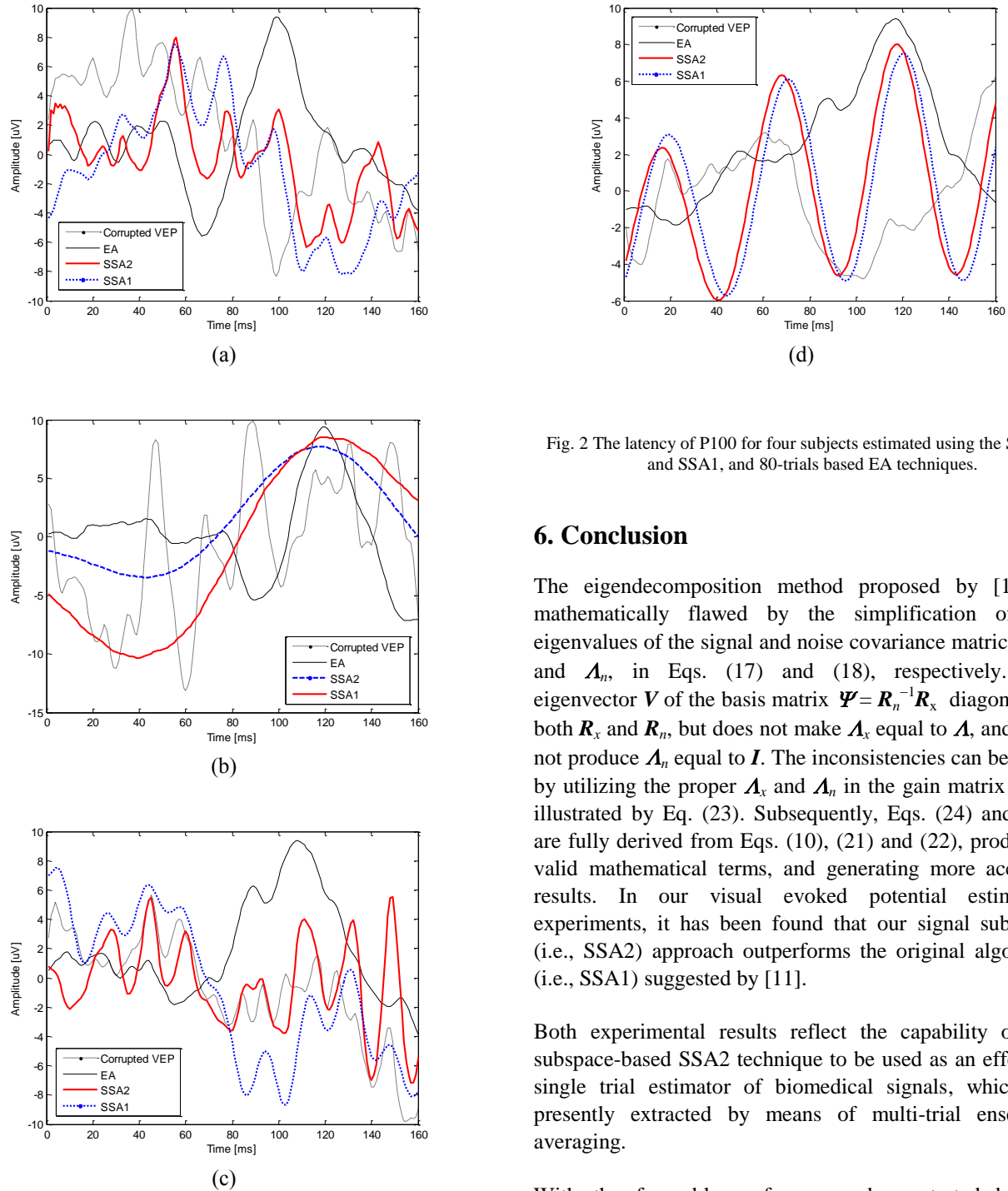


Fig. 2 The latency of P100 for four subjects estimated using the SSA2 and SSA1, and 80-trials based EA techniques.

6. Conclusion

The eigendecomposition method proposed by [11] is mathematically flawed by the simplification of the eigenvalues of the signal and noise covariance matrices, \mathbf{A}_x and \mathbf{A}_n , in Eqs. (17) and (18), respectively. The eigenvector \mathbf{V} of the basis matrix $\mathbf{\Psi} = \mathbf{R}_n^{-1} \mathbf{R}_x$ diagonalizes both \mathbf{R}_x and \mathbf{R}_n , but does not make \mathbf{A}_x equal to \mathbf{A} , and does not produce \mathbf{A}_n equal to \mathbf{I} . The inconsistencies can be fixed by utilizing the proper \mathbf{A}_x and \mathbf{A}_n in the gain matrix \mathbf{G} , as illustrated by Eq. (23). Subsequently, Eqs. (24) and (25) are fully derived from Eqs. (10), (21) and (22), producing valid mathematical terms, and generating more accurate results. In our visual evoked potential estimation experiments, it has been found that our signal subspace (i.e., SSA2) approach outperforms the original algorithm (i.e., SSA1) suggested by [11].

Both experimental results reflect the capability of the subspace-based SSA2 technique to be used as an effective single trial estimator of biomedical signals, which are presently extracted by means of multi-trial ensemble averaging.

With the favorable performance demonstrated by the outcome of the simulated and real patient data, SSA2 has the potentials to be used not only as biomedical signal estimators from the brain, but also as general purpose blind signal separators in any other fields where SNR values are relatively low. Among the fields which can benefit from the proposed algorithms include biology, communication, oil and gas, and agriculture.

Acknowledgments

We would like to thank Dr. Tara Mary George and Mr. Mohd Zawawi Zakaria of the Ophthalmology Department, Selayang Hospital, Kuala Lumpur for acquiring the VEP data.

References

- [1] F. Deprettere (ed.). *SVD and Signal Processing: Algorithms, Applications and Architectures*, North-Holland Publishing Co., 1989.
- [2] B. C. Levy. *Principles of Signal Detection and Parameter Estimation*, Springer Science+Business Media, LLC, New York, 2008.
- [3] Mohd Zuki Yusoff and Nidal Kamel, "A Time-Domain Subspace Technique for Estimating Evoked Potential Latencies," *International Journal of Computer Science and Network Security*, vol. 10, no. 1, pp. 144-153, January 2010.
- [4] R. Kumaresan and D. W. Tufts, "Estimating the Parameters of Exponentially Damped Sinusoids and Pole-Zero Modeling in Noise," *IEEE Transaction on Acoustics, Speech and Signal Processing*, 30(6): pp. 833-840, December 1982.
- [5] D. W. Tufts, R. Kumaresan and I. Kirsteins, "Data Adaptive Signal Estimation by Singular Value Decomposition of a Data Matrix," *Proceedings of the IEEE*, 70(6): pp. 684-685, June 1982.
- [6] S. Y. Kung, "A New Identification and Model Reduction Algorithm via SVD," the 12th Asilomar Conference on Circuits, Syst., Comput., pp. 705-714, Pacific Grove, CA, 1978.
- [7] P. van Overschee and B. De Moor. *Subspace Identification for Linear Systems*, Kluwer Academic Publishers, 1996.
- [8] Y. Ephraim and H. L. Van Trees, "A Signal Subspace Approach for Speech Enhancement," *IEEE Transaction on Speech and Audio Processing*, vol. 3, no. 4, pp. 251-266, July 1995.
- [9] Peter S. K. Hansen, "Signal Subspace Methods for Speech Enhancement," Ph.D. Thesis, IMM, Department of Mathematical Modelling, Technical University of Denmark, Lyngby, Denmark, 1997.
- [10] A. Rezayee and S. Gazor, "An Adaptive KLT Approach for Speech Enhancement," *IEEE Transactions on Speech and Audio Processing*, vol. 9, no. 2, pp. 87-95, February 2001.
- [11] Y. Hu and P. C. Loizou, "A Generalized Subspace Approach for Enhancing Speech Corrupted by Colored Noise," *IEEE Transactions on Speech and Audio Processing*, vol. 11, no. 4, pp. 334-341, July 2003.
- [12] S. Andrews, R. Palaniappan and N. Kamel, "Extracting Single Trial Visual Evoked Potentials using Selective Eigen-Rate Principal Components," *World Enformatika Society Transactions on Engineering, Computing and Technology*, vol. 7, pp. 330-333, August 2005.
- [13] X. H. Yu, Z. Y. He and Y. S. Zhang, "Time-Varying Adaptive Filters for Evoked Potential Estimation," *IEEE Transactions on Biomedical Engineering*, vol. 41, no. 11, pp. 1062-1071, November 1994.
- [14] A. Cichocki, R. R. Gharieb and T. Hoya, "Efficient Extraction of Evoked Potentials by Combination of Wiener Filtering and Subspace Methods", *IEEE Transactions on Biomedical Engineering*, pp. 3117-3120, 2001.
- [15] X. Xiong and Y. Chen, "Extracting ERP by Combination of Subspace Method and Lift Wavelet Transform," in *Proc. 27th Annual Conference of IEEE Engineering in Medicine and Biology Society (IEEE-EMBS 2005)*, Shanghai, China, September 1-4, 2005, pp. 5938-5941.



Mohd Zuki Yusoff is a lecturer at Universiti Teknologi PETRONAS, Malaysia. He received his BSc in Electrical Engineering in 1988 from Syracuse University, USA. He is a member of Tau Beta Pi, the National Engineering Honorary Society, and Eta Kappa Nu, the Electrical & Computer Engineering Honorary Society. He obtained an MSc in Communications, Networks & Software in 2001 from Surrey University, England. He received his PhD in Electrical & Electronic Engineering from Universiti Teknologi PETRONAS, Malaysia in 2009. Dr. Mohd Zuki's research interests include signal processing, embedded systems, and network management & control.



Fawnizu Azmadi Hussin is a senior lecturer at Universiti Teknologi PETRONAS, Malaysia. He obtained the Bachelor of Electrical Engineering, specializing in Computer Design from the University of Minnesota, Twin Cities, U.S.A. in 1999 and subsequently his M.Eng.Sc. in Systems and Control from the University of New South Wales, Australia in 2001. He completed his PhD in 2008 at the Nara Institute of Science and Technology in Japan under the scholarship from the Japanese Government (Monbukagakusho). Dr. Fawnizu's research interests are in VLSI design and test, especially in core-based testing, SOC and NOC. He is currently working on embedded and pervasive systems. He is also actively involved with the IEEE Malaysia Section and the IEEE Circuits and Systems Society in Malaysia.